Enzymatically Active Microgels from Self-Assembling Protein Nanofibrils for Microflow Chemistry

Xiao-Ming Zhou,[†,⊥,‡] Ulyana Shimanovich,[§,‡] Therese W. Herling,[§] Si Wu,[†] Christopher M. Dobson,[§] Tuomas P. J. Knowles,[*,§] and Sarah Perrett[*,†]

[†]National Laboratory of Biomacromolecules, Institute of Biophysics, Chinese Academy of Sciences, 15 Datun Road, Chaoyang District, Beijing 100101, China, [§]Department of Chemistry, University of Cambridge, Lensfield Road, Cambridge CB2 1EW, United Kingdom, and [⊥]University of the Chinese Academy of Sciences, 19A Yuquan Road, Shijingshan District, Beijing 100049, China. [‡]These authors contributed equally.

ABSTRACT

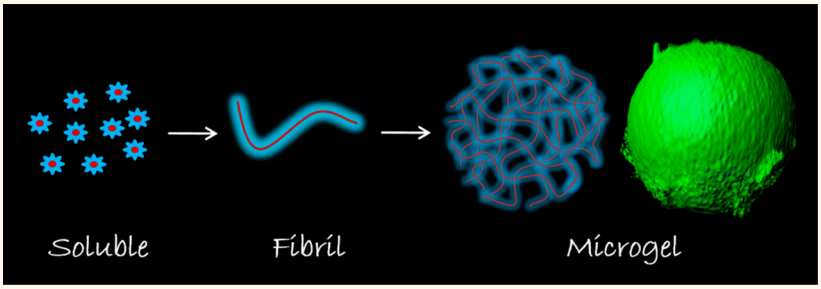

Amyloid fibrils represent a generic class of protein structure associated with both pathological states and with naturally occurring functional materials. This class of protein nanostructure has recently also emerged as an excellent foundation for sophisticated functional biocompatible materials including scaffolds and carriers for biologically active molecules. Protein-based materials offer the potential advantage that additional functions can be directly incorporated *via* gene fusion producing a single chimeric polypeptide that will both self-assemble and display the desired activity. To succeed, a chimeric protein system must self-assemble without the need for harsh triggering conditions which would damage the appended functional protein molecule. However, the micrometer to nanoscale patterning and morphological control of protein-based nanomaterials has remained challenging. This study demonstrates a general approach for overcoming these limitations through the microfluidic generation of enzymatically active microgels that are stabilized by amyloid nanofibrils. The use of scaffolds formed from biomaterials that self-assemble under mild conditions enables the formation of catalytic microgels while maintaining the integrity of the encapsulated enzyme. The enzymatically active microgel particles show robust material properties and their porous architecture allows diffusion in and out of reactants and products. In combination with microfluidic droplet trapping approaches, enzymatically active microgels illustrate the potential of self-assembling materials for enzyme immobilization and recycling, and for biological flow-chemistry. These design principles can be adopted to create countless other bioactive amyloid-based materials with diverse functions.

KEYWORDS: amyloid fibrils · Ure2 · alkaline phosphatase · microfluidics · enzymatic microgel

The intricate relationship between protein structure and function, which has been tuned by evolutionary pressures over many millenia, can serve as a fruitful source of inspiration for the design of functional materials with predictable behavior, and in recent years, new and increasingly complex protein-based functional materials have become readily available.[1−6] Controlling the supramolecular structure and, indeed, the conformation of individual peptide chains offers an opportunity to refine the properties of such materials in exquisite detail relative to other conventional biopolymers due to the high sensitivity of proteins to environmental changes which can lead, for example, to a wide variety of conformational transitions between the multiple states that can be adopted by proteins.[7,8] The creation of protein-based biomaterials which maintain high levels of enzymatic activity is a key requirement for successfully implementing enzymatic flow-chemistry.[9,10] This paper describes

* Address correspondence to sarah.perrett@cantab.net, tpjk2@cam.ac.uk.

Received for review January 5, 2015 and accepted June 1, 2015.

Published online June 01, 2015
10.1021/acsnano.5b00061

approaches to the control of enzymatic reactions within bioactive microgel scaffolds, where conversion of substrate into product may be regulated by diffusion-controlled catalysis. A microgel is a three-dimensional colloidal network of highly polymerized molecules of micrometer-scale size in which swelling of flexible particles occurs due to the incorporation of solvent molecules within its gel structure.[11,12] Given the advantages of size, porous architecture and desirable properties of the component molecules, microgels have been widely used in applications such as drug delivery,[13,14] microsensors[15] and biomaterials.[16,17]

Almost all of the structural materials explored for generating microgels to date have involved polymerization or cross-linking of synthetic molecules to allow gel formation.[17−19] The polymerization of many of these synthetic systems requires nonbiocompatible conditions or reagents, such as extreme pH, high temperature or exposure to highly reactive chemicals or to high doses of UV radiation.[20−26] There are, however, a very few examples where naturally occurring biological molecules have been utilized in the formation of biomicrogels, which include agarose,[27] chitosan,[28] and alginate.[29,30] As transporters of molecules of biological and medical importance, microgels have been functionalized with a wide range of compounds, including pharmaceuticals,[31,32] bioactive molecules[33−35] and living cells.[27,36] Although many polymerized molecules have been found to form microgels, biomedical applications require the use of species that are biocompatible.[37] In general, microgels composed from natural molecules can mimic biological environments more readily than those formed from synthetic compounds and also induce a lower immune response; it has been shown, for example, that a hydrogel formed from modified peptides can serve as a functional extracellular matrix.[38] Naturally occurring polymers of biomolecules, such as proteins, are thus excellent candidates for the investigation of novel biocompatible microgels. Protein-based materials offer the additional advantage that novel functions can be directly incorporated *via* gene fusion producing a single chimeric polypeptide that can potentially both self-assemble and display the desired activity.[10,39] However, finding suitable chimeric systems that will assemble under sufficiently mild conditions, and achieving controlled patterning of such nanomaterials, remains challenging.

In the present study, we have used amyloid fibrils as the structural component of the microgels. Amyloid fibrils are ubiquitous protein polymers, the formation of which is associated with a range of protein misfolding diseases,[40−42] but they can also play functional roles in organisms.[43−46] Due to the highly ordered β-sheet-rich structure in their cores, amyloid fibrils can be very stable, even under extreme conditions, and can be formed from a very wide range of peptides and proteins with highly variable chemical and physical properties. These properties, in combination with tunable assembly by control of *in vitro* conditions, such as pH and temperature, has motivated the exploration of amyloid fibrils as potential biomaterials.[10,47−53] One characteristic of amyloidogenic proteins is their ability to spontaneously self-propagate or self-assemble, often under mild conditions in aqueous solution, which means that polymerization into a stable fibrillar nanomaterial does not require additional cross-linking or other modifications.

In the present work, we have explored the amyloidogenic protein Ure2 as our structural material and produced functionalized microgels with enzymatic activity. The Ure2 protein is a regulator of nitrogen metabolism in the yeast *Saccharomyces cerevisiae*. It acts as a prion making it an excellent model for understanding the mechanism of prion propagation.[44] It readily forms amyloid fibrils *in vitro* and we have demonstrated that the prion domain of Ure2 can be used as a scaffold for self-immobilization and display of a variety of proteins in their bioactive forms when appended to the prion domain by genetic fusion.[10] Further, although a variety of established methods exist for preparing microgel particles,[14,54] we have used microfluidic techniques for making droplet-based microgels, because the size, morphology and monodispersity of the particles can be controlled with precision.[25,54] In addition to these advantages, the use of microfluidic techniques also has the potential for high-throughput applications.[27,55−57]

RESULTS AND DISCUSSION

We have used in this study a construct in which the enzyme alkaline phosphatase (AP) was genetically fused to the prion domain of Ure2 and displayed on the amyloid fibrils formed by self-assembly of this fused protein sequence. AP has a wide range of applications in the biological and clinical sciences, and its activity when displayed on the surface of an Ure2 prion domain fibril core has already been demonstrated and characterized, including measurement of enzyme kinetic parameters.[10] Here, solutions of Ure2-AP protein in soluble form were encapsulated into uniform 20-μm-sized droplets using microfluidic techniques. The encapsulated Ure2-AP then self-assembled into amyloid fibrils with the same rate and efficiency as the soluble protein in bulk solution. The resulting fibrils formed a three-dimensional network which incorporated water molecules to form uniform microgel spheres, resulting in the controlled immobilization of AP molecules. Measurement of the enzymatic behavior of the Ure2-AP microgel particles showed that the AP molecules retained enzymatic activity.

We used a carefully designed microfluidic droplet maker (Figure 1a) to generate the Ure2-AP microgels.

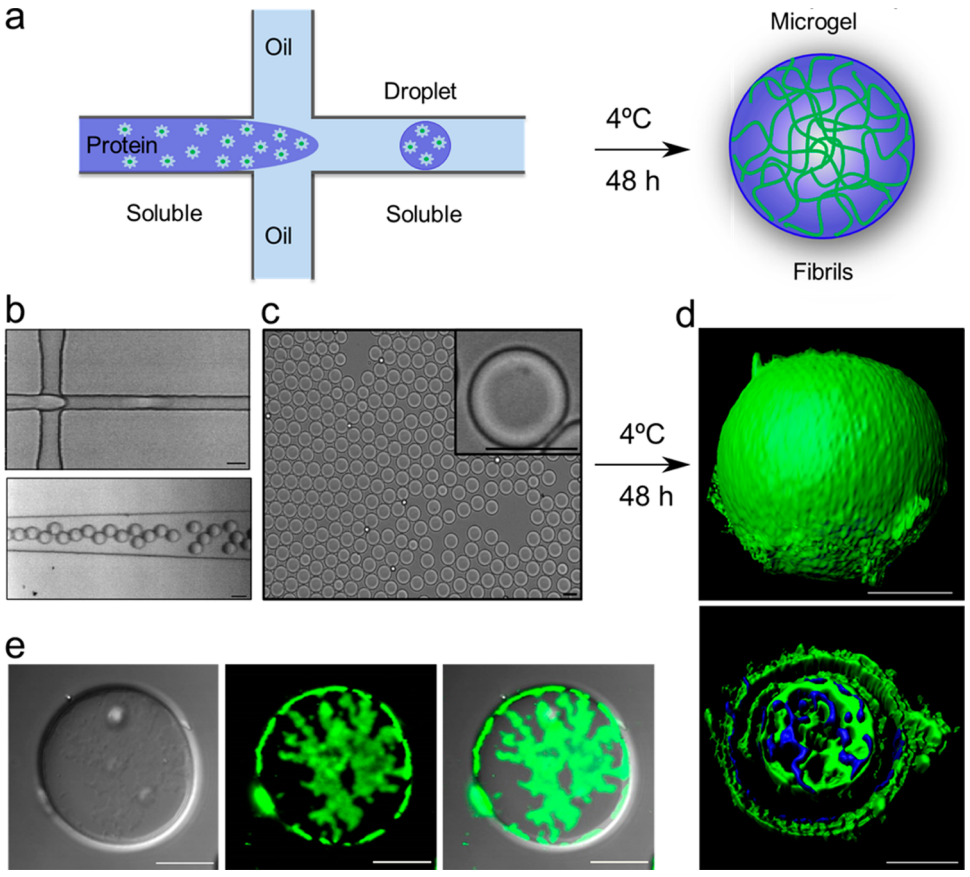

Figure 1. Demonstration of the principles of the approach used in the present work. (a) Schematic diagram of protein microgel formation. (b) Encapsulation of Ure2-AP droplets in microfluidic droplet-making device. The scale bars are 20 μm. (Upper panel) Droplet formation at the T-junction of the microfluidic channel. (Lower panel) Droplets inside the microfluidic channel. See also Supporting Information Video Files S1, corresponding to *upper panel*, and S2, corresponding to *lower panel*. (c) Uniformity of the resulting Ure2-AP droplets observed using light microscopy. Scale bars are 20 μm. (Inset) Enlarged image of a single microgel droplet. (d) Ure2-AP droplets after incubation to allow fibril formation, stained with the amyloid-specific fluorescent dye ThT and analyzed by confocal microscopy (see Methods). Green fluorescence indicates ThT bound to amyloid structure; blue fluorescence indicates free ThT. Scale bars are 10 μm. (Upper panel) Three-dimensional surface image. (Lower panel) Central cross-sectional image. (e) Ure2-GFP droplets after incubation to allow fibril formation, analyzed by confocal microscopy. Scale bars are 10 μm. (Left panel) Bright-field DIC image; (middle panel) GFP; (right panel) merged.

The soluble Ure2-AP chimeric protein (see Methods section) and Fluorinert oil were injected into the microfluidic channels using a hydrodynamic pump and made contact at the T junction of the channel device, where the protein solution dispersed into uniform droplets coated with Fluorinert oil (Figure 1a,b, Supporting Information Video Files S1 and S2). The resulting droplets showed a very high degree of uniformity in size as observed by light microscopy (Figures 1c and 2b, *left panel*). The droplets were generated at room temperature. The soluble Ure2-AP protein was then transformed into amyloid fibrils by incubation at 4 °C for 48 h (Figure 1a). These mild conditions for gel formation are compatible with the conservation of enzymatic activity, allowing the enzyme to be present before the microgel formation and thereby enabling us to achieve uniform catalytic activity throughout the gel structure. The formation of amyloid fibrils by the encapsulated Ure2-AP was initially confirmed by washing the microgel particles to remove the oil, then incubating with the amyloid-binding dye Thioflavin T (ThT) and observing its fluorescent properties. Confocal imaging showed the presence of ThT fluorescence within the microgel particles as well as at their surface (Figure 1d). As an additional approach to viewing the internal structure of the particles, another chimeric protein was constructed with green fluorescent protein (GFP) in place of AP and microgel particles were formed using the same protocol as for Ure2-AP. Again, cross-sectional images showed regions of intense fluorescence both at the surface and within the interior of the microgel particles (Figure 1e), consistent with the presence of protein fibrils throughout the microgel particles. Imaging the droplets using atomic force microscopy (AFM) and transmission electron microscopy (TEM) revealed a compact structural network of amyloid fibrils within the droplets (Figure 2), which is in good agreement with the observations from confocal microscopy analysis.

The structure of the Ure2-AP microgel droplets was further investigated by AFM and TEM. The droplets were disrupted by vortexing and high-speed centrifugation in order to release the Ure2-AP fibrils that then

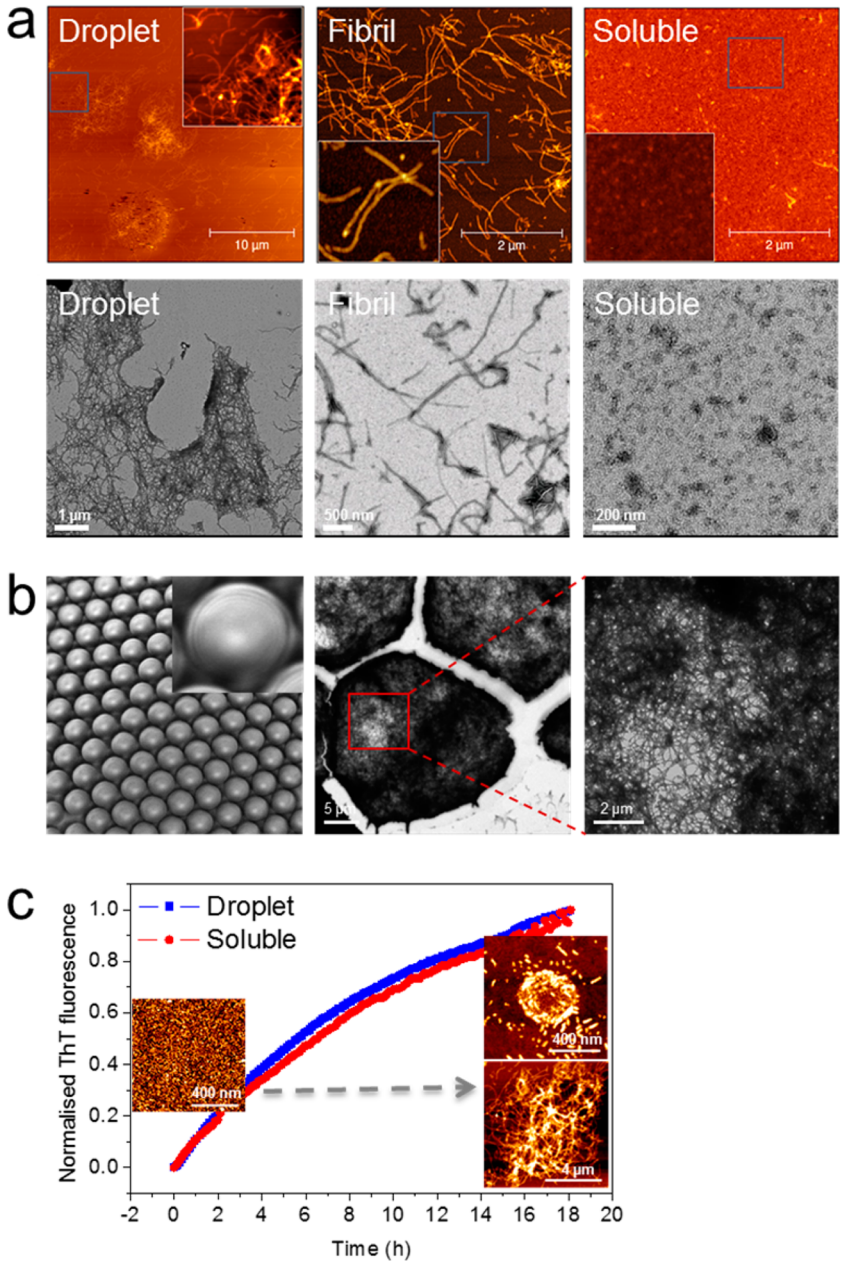

Figure 2. Microgel formation of Ure2-AP. (a) Analysis of Ure2-AP aggregates by AFM (upper panels) and negative stain TEM (lower panels). Ure2-AP droplet fragments (left panels) show a dense mesh-like network formed of amyloid fibrils similar to the individual fibrils formed in bulk solution (middle panels), whereas soluble Ure2-AP before incubation to form fibrils contains only small aggregates (right panels). (Insets) Enlarged scanning of boxed area in each AFM image. The scale bars are as indicated. (b) Droplets of Ure2-AP solution were formed as shown in Figure 1. Uniformity of the resulting droplets observed using light microscopy (left panel). Droplets were incubated to allow microgel formation (see Figure 1) and then intact droplets were added directly onto a nondischarged carbon-coated grid, stained, and imaged by TEM. Negatively stained droplets could be observed (middle panel), containing a dense network of amyloid fibrils within each droplet (right panel). (c) The kinetics of fibril assembly for encapsulated Ure2-AP and for Ure2-AP in bulk solution were monitored by ThT binding fluorescence. (Insets) AFM images demonstrate the conversion of droplet-encapsulated Ure2-AP from the soluble to the fibrillar state. The scale bars are as indicated.

became partially dispersed (Figure 2a), and the fibrillar network within a single droplet can be observed in the AFM or negative stain TEM images (Figure 2a, *left panels*). The images of the Ure2-AP fibrils formed in bulk solution (without oil encapsulation) under the same conditions reveal well dispersed fibrils, without spherical structures or highly condensed packing of fibrils (Figure 2a, *middle panels*). In addition, solutions of the soluble Ure2-AP used for making the droplets show no evidence for large fibrillar aggregates, although a few small rod-like assemblies could be observed, which may represent structures formed prior to the experiments (Figure 2a, *right panels*). The network of fibrils within intact Ure2-AP droplets was further

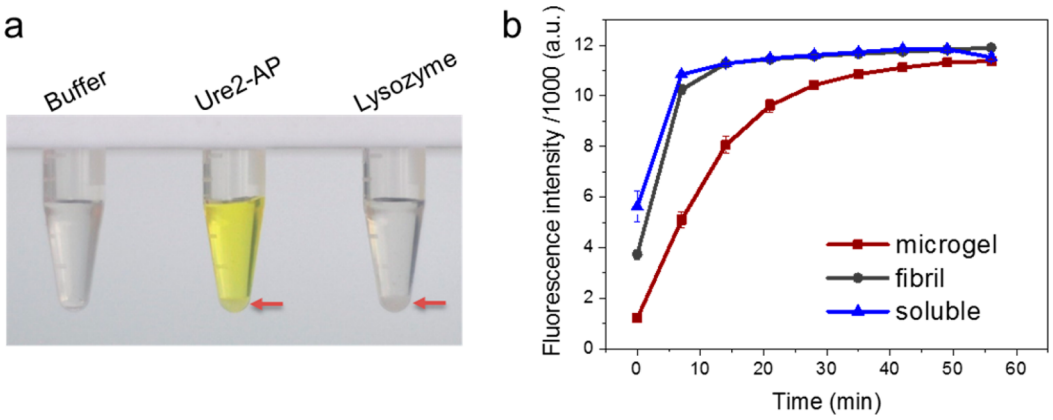

Figure 3. Enzyme activity determination of Ure2-AP microgel particles. (a) Ure2-AP microgel particles, lysozyme microgel particles and Buffer A, as indicated, were each incubated with BBTP substrate at room temperature for 2 h. Stable microgel particles at the bottom of the Eppendorf tube are indicated by *red arrows*. The fluorescent substrate BBTP is colorless in the visible range, but its product BBT is yellow. (b) Production of the fluorescent product BBT was used to monitor the activity of Ure2-AP microgel particles, Ure2-AP fibrils, and soluble Ure2-AP, as indicated. Measurements were performed in a BMG FLUOstar Omega plate reader. Error bars represent the standard error of the mean of at least three measurements.

investigated by placing intact droplets directly onto the hydrophobic surface of nondischarged carbon-coated TEM sample grids (Figure 2b, *middle and right panels*), supporting the conclusion that the microgel particles are formed from an intertwined network of fibrils.

The kinetics of WT Ure2 fibril formation has previously been analyzed in detail and monitoring of ThT fluorescence was shown to reliably reflect the extent of fibril formation,[58] and can also shed light on the influence of internal and external factors on the rates of individual molecular steps in the fibril formation process.[58−61] Like WT Ure2,[58,62] the assembly of Ure2-AP fibrils is highly efficient, proceeding essentially to completion, and the fibrils are stable even to repeated dilution or washing in buffer.[10] The kinetics of fibril formation were studied for both droplet-encapsulated Ure2-AP and Ure2-AP in bulk solution by analyzing the time dependence of the ThT fluorescence. The encapsulated and free chimeric protein showed similar kinetic behavior (Figure 2c), reflecting the transition from the soluble to fibrillar state (shown by AFM for the droplet sample, Figure 2c *insets*). As noted above (Figure 1c), the majority of droplet particles are around 20 μm in diameter, and the fibrils dispersed from these particles were estimated to be at least 2 μm in length (Figure 2a, *left panels* and Figure 2c, *lower right inset*), similar to the fibrils formed in free solution (Figure 2a, *middle panels*), which is consistent with the similarity in kinetic behavior. Occasionally, smaller droplets of about 400 nm in diameter were found to be stable toward the disruption process (Figure 2c, *upper right inset*), where the Ure2-AP appears as short fibrils of length 40−100 nm. This observation we attribute to the geometrical constraints of the droplet environment. These results are consistent with formation of a fibrillar network by highly efficient self-assembly of the chimeric Ure2-AP protein encapsulated within the droplet, leading to microgel particle formation. Further, the fibril assembly mechanism within the droplets appears to be indistinguishable from that in bulk solution.

The enzymatic activity of the Ure2-AP fibrils within the microgel droplets was monitored using the fluorescent substrate 2′-[2-benzothiazoyl]-6′-hydroxybenzothiazole phosphate (BBTP). The excitation and emission wavelengths are 340 and 440 nm, respectively, for BBTP, and 440 and 580 nm, respectively, for the product BBT following cleavage of the phosphate group by the enzyme; indeed, in the visible range, the substrate is colorless, whereas the product is yellow (Figure 3a). The substantial difference between the emission wavelengths of substrate and product allows independent detection of the two reaction components. The oil coating was first removed by washing (with Buffer A, see Methods) to allow the substrate to enter the droplets, and the enzyme activity of the Ure2-AP microgel particles was indicated by a rapid increase in the BBT product signal when the washed microgel particles were incubated with BBTP (Figure 3b). The rates of enzyme activity for soluble Ure2-AP and for Ure2-AP fibrils in bulk solution are almost identical, whereas the microgel particles showed a modest reduction in the rate of enzyme activity (Figure 3b). It is not unlikely that the microgel structure, containing a highly compact network of fibrils, reduces the rate of diffusion of the substrate and product to and from the enzyme. An increase in the diffusion barrier could in fact provide a practical advantage in applications of these microgel particles where slow release of payloads carried within the porous mesh of the microgel is desirable.[19,63] However, the relatively modest effect on rates indicates that substrate and product have ready access to the AP molecules displayed on the fibrillar network within the microgel particles, consistent with the structure of the particles as an aqueous microgel stabilized by a porous

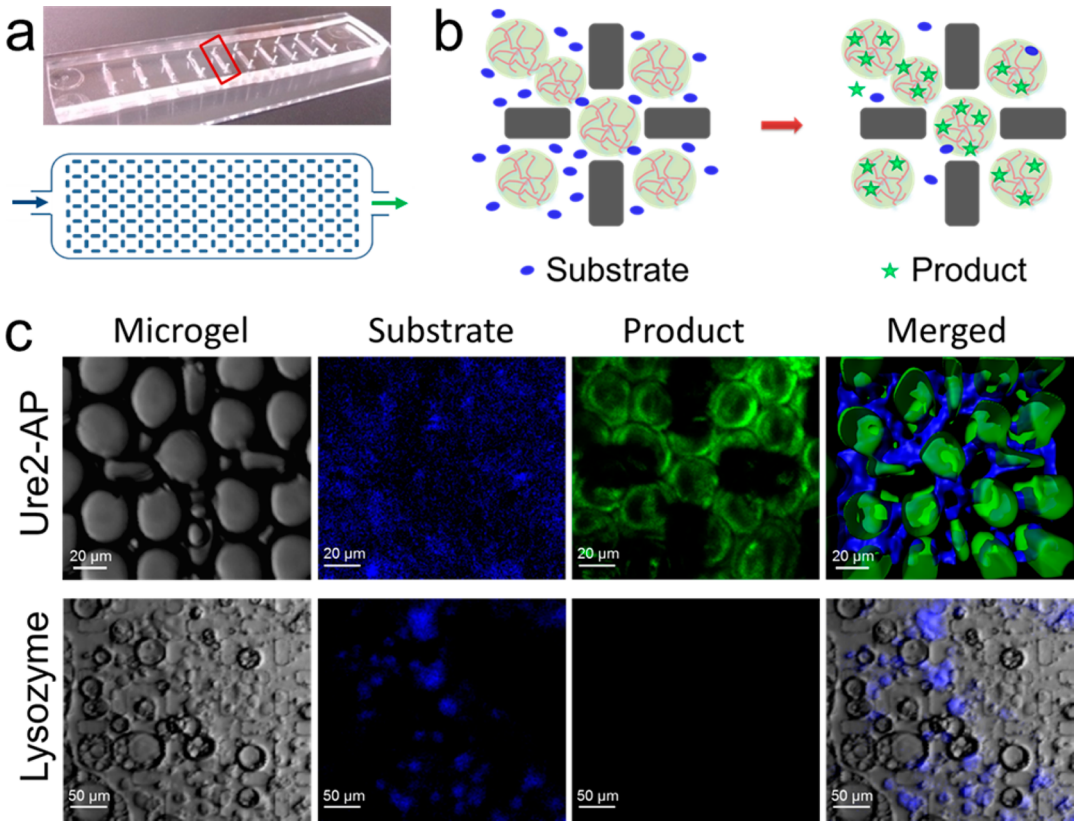

Figure 4. Droplet trapping device and distribution of fluorescent substrate and product. (a) Diagram (lower panel) showing the structure of the droplet trapping device fabricated from PDMS indicated in the photograph (upper panel) by a red box. (b) Schematic diagram of enzymatic activity of trapped Ure2-AP microgel particles in the droplet trapping device. Substrate flows into the device by hydrodynamic pumping and diffuses into the trapped Ure2-AP microgel particles where the substrate is efficiently catalyzed to the product by the fibril-displayed AP. (c) (Upper panel) Observation of trapped Ure2-AP microgel particles by bright-field DIC (far left). Fluorescence of substrate (blue) and product (green) after pumping substrate into the trapping device (middle panels). The three-dimensional microgel particles and the fluorescence of the substrate and product were reconstructed from serial two-dimensional scans by confocal microscopy (far right). Scale bars are 20 μm. (Lower panel) As a control, lysozyme microgel particles, which were preincubated with AP fluorescent substrate BBTP, were also trapped in the trapping device and observed under the confocal microscope. Substrate fluorescence is observed, but there is no conversion to product. Scale bars are 50 μm.

network of amyloid fibrils. Further, the results are consistent with previous measurement of enzyme kinetic parameters for Ure2-AP, which shows similar values for both k_{cat} and K_m for the soluble and fibrillar forms of the chimeric protein, suggesting that the activity of Ure2-AP is not greatly perturbed by diffusion barriers induced by fibril formation; this is in contrast to similar chimeras formed from another enzyme, horseradish peroxidase, which has a very high turnover number so that the rate of catalysis is essentially diffusion controlled, and thus the more substantial drop in activity on fibril formation reflects its greater sensitivity to steric hindrance.[10]

To visualize the enzymatic activity of the microgels and explore their potential application in microflow chemistry, we performed microfluidic bioactivity assays on the microgels. A microfluidic device was designed for this purpose (Figure 4a). The micropillar arrays in the device architecture created compartments for the trapping of individual microgels. The catalytic microgels were then retained within the microfluidic channel and supplied with a continuous flow of substrate (Figure 4b). This assay allowed us to achieve spatial resolution of the substrate distribution and the product formation within the enzymatic microgels (Figure 4c).

The size of the compartments was controlled by varying the distance between the micropillars and thereby customizing the arrays to trap droplets of different sizes. In our experiments, we trapped 20 μm (diameter) enzymatic microgel particles and flowed in substrate by hydrodynamic pumping. The substrate diffused into the trapped enzymatic microgels and the reaction was catalyzed to form the fluorescent product, which is schematically represented in Figure 4b. We observed the distribution of the fluorescent BBTP substrate and its conversion to fluorescent BBT product within the trapping device using confocal microscopy imaging. The microgel particles can be observed as luminous spheres with green product fluorescence and surrounded by the blue substrate fluorescence (Figure 4c, *upper panel*). As a control, we also trapped lysozyme microgels preincubated with the AP substrate

in the droplet trapping device. Under confocal microscopy, the lysozyme microgel particles emitted blue fluorescence due to the presence of the substrate, but no product fluorescence was observed (Figure 4c, *lower panel*), showing that the enzymatic activity obtained is specific to the presence of active AP molecules displayed on the nanofibril surface within the Ure2-AP microgel.

CONCLUSION

In conclusion, we have in the present study explored the suitability of the amyloidogenic protein Ure2 as a self-assembling material for microgel formation. We synthesized Ure2 microgels biofunctionalized with AP enzyme *via* genetic fusion, which is a model system that can be readily adapted to incorporate and thus immobilize other enzymes or bioactive proteins.[10] Amyloid-based microgels provide significant advantages over fibril formation in free solution. The application of microfluidics allows controlled formation of uniformly sized droplets. Thus, the amount of protein trapped in each homogeneous microgel particle is likewise uniform. The microgel particles are readily manipulated and can be collected in a trapping device. As demonstrated here, this provides a convenient method for enzyme immobilization, which is an important strategy for many industrial and clinical assays.[64,65] Microgel particles can also be used for slow release or targeted delivery of drugs and other bioactive molecules, as well as biosensors or biomaterials,[15,17,19,63] and when combined with the power of microfluidic techniques, can also be applied in high-throughput screening and microscale analytical techniques.[66−68] Thus, the enzymatic microgels described in this study illustrate the potential of self-assembling materials for biological flow-chemistry.

METHODS

Materials. Unless otherwise stated, reagents were purchased from Sigma-Aldrich. The Ure2-AP concentration was determined by the absorbance at 280 nm using an extinction coefficient of 33 140 $M^{-1}cm^{-1}$.

Protein Expression and Purification. The method of expressing and purifying Ure2-AP was as described previously.[10] In brief, Ure2-AP was expressed in C41 *Escherichia coli*, and the cells were grown at 37 °C to an optical density at 600 nm of 0.6, induced with 0.4 mM Isopropyl β-D-1-thiogalactopyranoside (IPTG) and grown at 16 °C for 20 h. The cells were lysed in Buffer A (50 mM Tris-HCl, 150 mM NaCl, pH 8.0), and the soluble Ure2-AP was applied to nickel affinity chromatography resin and purified according to the manufacturer's guidelines. Imidazole was removed from the purified proteins by buffer exchange into Buffer A, and the final protein was flash frozen with liquid nitrogen and stored at −80 °C.

The Ure2-GFP fusion protein was constructed, expressed, and purified in the same way as Ure2-AP but was stored in Buffer B (50 mM Tris-HCl, 150 mM NaCl, pH 7.4). The GFP gene was a kind gift from Pingsheng Liu (IBP, CAS).

Microfluidic Device Fabrication. Standard soft lithography techniques were used to fabricate the microfluidic devices, as described previously.[69,70] The microfluidic channels were patterned into polydimethylsiloxane (PDMS; Sylgard184, Dow Corning) using SU-8 photoresist (SU8-3025 Microchem) on silicon masters. The PDMS device was then plasma bonded using an oxygen plasma (Diener Electronics) to glass microscope slides to make a sealed device. The microfluidic channels of the droplet maker were washed with Aquapel and used to generate uniform droplets of 20 μm in diameter. The device for trapping the microdroplets was fabricated in the same way and contained a 1 mm × 5 mm × 0.02 mm chamber, with a calculated volume of less than 0.1 μL.

Droplet and Microgel Formation. Ure2-AP was defrosted from −80 °C and centrifuged at 15 000 rpm (Centrifuge 5424, Eppendorf) for 10 min, and the supernatant was transferred to a new tube. Soluble Ure2-AP was diluted to 35 μM in Buffer A and used to form droplets using a microfluidic droplet making device. The Ure2-AP and Fluorinert oil (containing 2% (w/v) *N*, *N*′-bis (*n*-propyl) poly(ethylene oxide)-bis (2-trifluoromethyl polyperfluoroethylene oxide)amide surfactant) were hydrodynamically pumped (Nemyses pump) into microfluidic channels at a flow rate of 150−200 μL/h and collided at the T-junction of the device. The Ure2-AP droplets coated with the oil were collected from the outlet of the microfluidic device at room temperature. The morphological uniformity of the resulting droplets was checked by light microscopy. The resulting droplets were incubated at 4 °C for 2 days. Free Ure2-AP was incubated under the same conditions as droplet-encapsulated Ure2-AP, as a comparison control. Ure2-GFP droplets and microgel particles were formed in the same way as Ure2-AP, except that 28 μM of protein in Buffer B was used.

For determination of fibril formation kinetics, soluble Ure2-AP (∼35 μM) mixed with 40 μM ThT was used to form droplets at room temperature. Then, the droplets and free Ure2-AP were loaded into 96 well plates (80 μL per well) and fibril formation was monitored at 30 °C for 18 h using a microplate reader (FLUOstar Omega, BMG), with excitation at 450 nm and emission at 485 nm.

For lysozyme microgel formation, 6% (w/w) lysozyme was dissolved in 20 mM HCl and 19.5 mM NaCl, and with Fluorinert oil, was pumped in microfluidic channels to form uniform droplets. The resulting lysozyme droplets were then incubated at 65 °C for 24 h to promote gelation.[53]

Atomic Force Microscopy (AFM). Ure2-AP microgel particles (100 μL) were suspended in 100 μL of Buffer A by mild vortexing, followed by centrifugation at 1000 rpm (Centrifuge 5424, Eppendorf) for 1 min. The oil and extra buffer were removed after centrifugation. The washed microgel particles were then resuspended in 100 μL of Buffer A and broken by fierce vortexing followed by centrifugation at 5000 rpm (Centrifuge 5424, Eppendorf) for 5 min at least twice. The control Ure2-AP fibrils formed from free protein (without oil encapsulation) were washed once and resuspended in Buffer A, as described previously.[10]

A 20 μL volume of soluble Ure2-AP, fibrillar Ure2-AP or disrupted Ure2-AP droplets, whose concentration was ∼35 μM, was dropped onto a fresh mica surface and allowed to stand for 2 min. The mica was then washed with deionized water and dried with nitrogen gas. The AFM images were taken by AFM (H-02-0067 NanoWizard II, JPK Instruments).

Transmission Electron Microscopy (TEM). For negative staining TEM, 6 μL drops of microgel particles were loaded onto glow-discharged carbon−coated grid (highly hydrophilic surface) or nondischarged carbon-coated grid (hydrophobic surface) for 1 min and blotted with filter paper to remove extra sample, then rinsed with 6 μL of deionized water and stained with 2% uranyl acetate for 20 s. Micrographs were recorded on a CM120-FEG (FEI) microscope operating at 100 kV.

Enzymatic Activity Assay. The microgel particles were washed with an equal volume of Buffer A by mild vortexing followed by centrifugation at 800 rpm (Centrifuge 5424, Eppendorf) for 1 min. (In order to determine the efficiency of conversion into

microgel particles, and to confirm that the microgel particles were stable during the washing process, the amount of protein released into the supernatant was measured and calculated as a fraction of total protein after each round of washing. The amount of protein that failed to form microgel particles and was removed in the initial 1 to 3 rounds of 1:1 washing equated to a fraction of around 10% of the total protein used. However, the well-formed microgel particles containing the remaining 90% of total protein were extremely stable in subsequent rounds of washing, and the fraction of protein released from the droplets at each subsequent round was less than 1%.) Ure2-AP fibrils were washed with buffer by centrifugation at 6000 rpm (Centrifuge 5424, Eppendorf) for 10 min and resuspended in Buffer A. The soluble Ure2-AP and Ure2-AP fibrils were diluted to a concentration of 35 μM.

Ure2-AP microgel particles, Ure2-AP fibrils and soluble Ure2-AP were each loaded into 96 well plates (1 μL per well) and mixed with 140 μL of 2′-(2-benzothiazoyl)-6′-hydroxybenzothiazole phosphate (BBTP, AttoPhos AP Fluorescent Substrate System, Promega) per well. The decrease in the fluorescent substrate and increase of fluorescent product were monitored using a microplate reader (FLUOstar Omega, BMG) with excitation at 334 nm and emission at 440 nm for substrate, and excitation at 440 nm and emission at 590 nm for product.

The same volumes (10 μL) of lysozyme microgel particles, Ure2-AP microgel particles and Buffer A were loaded at the bottom of an Eppendorf tube and incubated with 500 μL of BBTP substrate for 2 h at room temperature to confirm the activity and stability of enzymatic microgel particles.

Droplet Trapping. Ure2-AP microgel spheres were loaded into the droplet trapping device by syringe injection and trapped within subspaces of the device. Lysozyme microgel particles which had been preincubated with BBTP substrate for 15 min were trapped in the device in the same way.

Confocal Microscopy. Ure2-AP microgel particles were washed with Buffer A as described above. The washed microgel (100 μL) was incubated with 200 μL of ThT (40 μM) for 4 h, washed again in order to remove free dye, and then the ThT fluorescence of the microgel particles was observed by confocal microscopy (Laser Scan Leica SP2 microscope) using the tunable Argon 458/477/488/514 nm laser at 30 mW (for green excitation) and UV 405 nm laser at 25 mW (for violet excitation), with a 30 nm emission bandwidth. (The excitation/emission maxima for ThT bound to amyloid material are 450 nm/490 nm and for free ThT are 385 nm/445 nm.) The three-dimensional ThT fluorescent microgel sphere was reconstructed from two-dimensional serial scans (in average 150 z-stacks per single microgel particle) using Imaris 7.0 (Bitplane) image analysis software.

The BBTP substrate was pumped into the device in which Ure2-AP microgel particles were already trapped. The localization of fluorescent BBTP (excitation/emission maxima at 340 nm/440 nm) and reaction product BBT (excitation/emission maxima at 440 nm/580 nm) within the trapping device was observed by confocal microscopy (as described above, using a He/Cd 325 nm laser for UV excitation). Trapped lysozyme microgel particles were also observed and imaged under the same imaging conditions as Ure2-AP microgel particles.

Ure2-GFP microgel particles were washed with Buffer B and then 6 μL of the washed microgel was dropped onto a glass slide and covered with a coverslip. The images were obtained using an Olympus FV500 confocal microscope. The excitation and emission wavelengths for GFP imaging were 488 and 509 nm, respectively.

Conflict of Interest: The authors declare no competing financial interest.

Acknowledgment. We thank Thomas Müller (Department of Chemistry, University of Cambridge, U.K.) for assistance with optical microscopy. We thank Yanxia Jia (Center for Biological Imaging, IBP, CAS) for assistance with TEM experiments and Yang Wang (IBP, CAS) for assistance with confocal imaging. We thank Pingsheng Liu (IBP, CAS) for helpful discussions and access to equipment. S.P. acknowledges support from the Chinese Ministry of Science 973 Program [2012CB911000, 2013CB910700] and the National Natural Science Foundation of China [31110103914, 31070656, 31100564]. Work in the Knowles laboratory is supported by Elan Pharmaceuticals, the ERC, the BBSRC, and the Frances and Augustus Newman Foundation.

Supporting Information Available: Videos of droplet formation corresponding to the images shown in Figure 1b. The Supporting Information is available free of charge on the ACS Publications website at DOI: 10.1021/acsnano.5b00061.

REFERENCES AND NOTES

1. Zhang, S. G. Fabrication of Novel Biomaterials through Molecular Self-Assembly. *Nat. Biotechnol.* **2003**, *21*, 1171–1178.
2. Woolfson, D. N.; Mahmoud, Z. N. More Than Just Bare Scaffolds: Towards Multi-Component and Decorated Fibrous Biomaterials. *Chem. Soc. Rev.* **2010**, *39*, 3464–3479.
3. Grove, T. Z.; Regan, L. New Materials from Proteins and Peptides. *Curr. Opin. Struct. Biol.* **2012**, *22*, 451–456.
4. Li, C. X.; Mezzenga, R. The Interplay between Carbon Nanomaterials and Amyloid Fibrils in Bio-Nanotechnology. *Nanoscale* **2013**, *5*, 6207–6218.
5. Shimanovich, U.; Bernardes, G. J. L.; Knowles, T. P. J.; Cavaco-Paulo, A. Protein Micro- and Nano-Capsules for Biomedical Applications. *Chem. Soc. Rev.* **2014**, *43*, 1361–1371.
6. Adler-Abramovich, L.; Gazit, E. The Physical Properties of Supramolecular Peptide Assemblies: From Building Block Association to Technological Applications. *Chem. Soc. Rev.* **2014**, *43*, 6881–6893.
7. Dobson, C. M. Protein Folding and Misfolding. *Nature* **2003**, *426*, 884–890.
8. Chiti, F.; Dobson, C. M. Protein Misfolding, Functional Amyloid, and Human Disease. *Annu. Rev. Biochem.* **2006**, *75*, 333–366.
9. Bai, S.; Debnath, S.; Gibson, K.; Schlicht, B.; Bayne, L.; Zagnoni, M.; Ulijn, R. V. Biocatalytic Self-Assembly of Nanostructured Peptide Microparticles Using Droplet Microfluidics. *Small* **2014**, *10*, 285–293.
10. Zhou, X. M.; Entwistle, A.; Zhang, H.; Jackson, A. P.; Mason, T. O.; Shimanovich, U.; Knowles, T. P. J.; Smith, A. T.; Sawyer, E. B.; Perrett, S. Self-Assembly of Amyloid Fibrils That Display Active Enzymes. *ChemCatChem* **2014**, *6*, 1961–1968.
11. Funke, W.; Okay, O.; Joos-Muller, B. Microgels—Intramolecularly Crosslinked Macromolecules with a Globular Structure. *Adv. Polym. Sci.* **1998**, *136*, 139–234.
12. Das, M.; Zhang, H.; Kumacheva, E. Microgels: Old Materials with New Applications. *Annu. Rev. Mater. Res.* **2006**, *36*, 117–142.
13. Vinogradov, S. V. Colloidal Microgels in Drug Delivery Applications. *Curr. Pharm. Des.* **2006**, *12*, 4703–4712.
14. Oh, J. K.; Drumright, R.; Siegwart, D. J.; Matyjaszewski, K. The Development of Microgels/Nanogels for Drug Delivery Applications. *Prog. Polym. Sci.* **2008**, *33*, 448–477.
15. Hu, Z. B.; Chen, Y. Y.; Wang, C. J.; Zheng, Y. D.; Li, Y. Polymer Gels with Engineered Environmentally Responsive Surface Patterns. *Nature* **1998**, *393*, 149–152.
16. Jia, X. Q.; Yeo, Y.; Clifton, R. J.; Jiao, T.; Kohane, D. S.; Kobler, J. B.; Zeitels, S. M.; Langer, R. Hyaluronic Acid-Based Microgels and Microgel Networks for Vocal Fold Regeneration. *Biomacromolecules* **2006**, *7*, 3336–3344.
17. Saunders, B. R.; Laajam, N.; Daly, E.; Teow, S.; Hu, X. H.; Stepto, R. Microgels: From Responsive Polymer Colloids to Biomaterials. *Adv. Colloid Interface Sci.* **2009**, *147−48*, 251–262.
18. Saunders, B. R.; Vincent, B. Microgel Particles as Model Colloids: Theory, Properties and Applications. *Adv. Colloid Interface Sci.* **1999**, *80*, 1–25.
19. Hoare, T. R.; Kohane, D. S. Hydrogels in Drug Delivery: Progress and Challenges. *Polymer* **2008**, *49*, 1993–2007.
20. Nolan, C. M.; Reyes, C. D.; Debord, J. D.; Garcia, A. J.; Lyon, L. A. Phase Transition Behavior, Protein Adsorption, and Cell Adhesion Resistance of Poly(ethylene glycol) Cross-Linked Microgel Particles. *Biomacromolecules* **2005**, *6*, 2032–2039.

21. Kim, K. S.; Vincent, B. Ph and Temperature-Sensitive Behaviors of Poly(4-vinyl pyridine-co-N-isopropyl acrylamide) Microgels. *Polym. J.* **2005**, *37*, 565–570.
22. Seiffert, S.; Oppermann, W.; Saalwaechter, K. Hydrogel Formation by Photocrosslinking of Dimethylmaleimide Functionalized Polyacrylamide. *Polymer* **2007**, *48*, 5599–5611.
23. Li, Z. F.; Ming, T.; Wang, J. F.; Ngai, T. High Internal Phase Emulsions Stabilized Solely by Microgel Particles. *Angew. Chem., Int. Ed.* **2009**, *48*, 8490–8493.
24. Kanai, T.; Lee, D.; Shum, H. C.; Shah, R. K.; Weitz, D. A. Gel-Immobilized Colloidal Crystal Shell with Enhanced Thermal Sensitivity at Photonic Wavelengths. *Adv. Mater.* **2010**, *22*, 4998–5002.
25. Seiffert, S.; Romanowsky, M. B.; Weitz, D. A. Janus Microgels Produced from Functional Precursor Polymers. *Langmuir* **2010**, *26*, 14842–14847.
26. Ma, S. H.; Thiele, J.; Liu, X.; Bai, Y. P.; Abell, C.; Huck, W. T. S. Fabrication of Microgel Particles with Complex Shape *via* Selective Polymerization of Aqueous Two-Phase Systems. *Small* **2012**, *8*, 2356–2360.
27. Kumachev, A.; Greener, J.; Tumarkin, E.; Eiser, E.; Zandstra, P. W.; Kumacheva, E. High-Throughput Generation of Hydrogel Microbeads with Varying Elasticity for Cell Encapsulation. *Biomaterials* **2011**, *32*, 1477–1483.
28. Agnihotri, S. A.; Mallikarjuna, N. N.; Aminabhavi, T. M. Recent Advances on Chitosan-Based Micro- and Nanoparticles in Drug Delivery. *J. Controlled Release* **2004**, *100*, 5–28.
29. Augst, A. D.; Kong, H. J.; Mooney, D. J. Alginate Hydrogels as Biomaterials. *Macromol. Biosci.* **2006**, *6*, 623–633.
30. Tan, W. H.; Takeuchi, S. Monodisperse Alginate Hydrogel Microbeads for Cell Encapsulation. *Adv. Mater.* **2007**, *19*, 2696–2701.
31. Vinogradov, S. V.; Bronich, T. K.; Kabanov, A. V. Nanosized Cationic Hydrogels for Drug Delivery: Preparation, Properties and Interactions with Cells. *Adv. Drug Delivery Rev.* **2002**, *54*, 135–147.
32. Lopez, V. C.; Hadgraft, J.; Snowden, M. J. The Use of Colloidal Microgels as a (Trans)Dermal Drug Delivery System. *Int. J. Pharm.* **2005**, *292*, 137–147.
33. Peters, M. C.; Isenberg, B. C.; Rowley, J. A.; Mooney, D. J. Release from Alginate Enhances the Biological Activity of Vascular Endothelial Growth Factor. *J. Biomater. Sci., Polym. Ed.* **1998**, *9*, 1267–1278.
34. Mao, H. Q.; Roy, K.; Troung-Le, V. L.; Janes, K. A.; Lin, K. Y.; Wang, Y.; August, J. T.; Leong, K. W. Chitosan-DNA Nanoparticles as Gene Carriers: Synthesis, Characterization and Transfection Efficiency. *J. Controlled Release* **2001**, *70*, 399–421.
35. Retama, J. R.; Lopez-Ruiz, B.; Lopez-Cabarcos, E. Microstructural Modifications Induced by the Entrapped Glucose Oxidase in Cross-Linked Polyacrylamide Microgels Used as Glucose Sensors. *Biomaterials* **2003**, *24*, 2965–2973.
36. Velasco, D.; Tumarkin, E.; Kumacheva, E. Microfluidic Encapsulation of Cells in Polymer Microgels. *Small* **2012**, *8*, 1633–1642.
37. Wang, Y. X.; Robertson, J. L.; Spillman, W. B.; Claus, R. O. Effects of the Chemical Structure and the Surface Properties of Polymeric Biomaterials on Their Biocompatibility. *Pharm. Res.* **2004**, *21*, 1362–1373.
38. Mi, L. X.; Fischer, S.; Chung, B.; Sundelacruz, S.; Harden, J. L. Self-Assembling Protein Hydrogels with Modular Integrin Binding Domains. *Biomacromolecules* **2006**, *7*, 38–47.
39. Huang, Z.; Salim, T.; Brawley, A.; Patterson, J.; Matthews, K. S.; Bondos, S. E. Functionalization and Patterning of Protein-Based Materials Using Active Ultrabithorax Chimeras. *Adv. Funct. Mater.* **2011**, *21*, 2633–2640.
40. Kelly, J. W. Alternative Conformations of Amyloidogenic Proteins Govern Their Behavior. *Curr. Opin. Struct. Biol.* **1996**, *6*, 11–17.
41. Sunde, M.; Blake, C. The Structure of Amyloid Fibrils by Electron Microscopy and X-Ray Diffraction. *Adv. Protein. Chem.* **1997**, *50*, 123–159.
42. Kelly, J. W. The Alternative Conformations of Amyloidogenic Proteins and Their Multi-Step Assembly Pathways. *Curr. Opin. Struct. Biol.* **1998**, *8*, 101–106.
43. Olsen, A.; Jonsson, A.; Normark, S. Fibronectin Binding Mediated by a Novel Class of Surface Organelles on *Escherichia coli*. *Nature* **1989**, *338*, 652–655.
44. Wickner, R. B. [Ure3] as an Altered Ure2 Protein: Evidence for a Prion Analog in Saccharomyces Cerevisiae. *Science* **1994**, *264*, 566–569.
45. Sawyer, E. B.; Claessen, D.; Gras, S. L.; Perrett, S. Exploiting Amyloid: How and Why Bacteria Use Cross-Beta Fibrils. *Biochem. Soc. Trans.* **2012**, *40*, 728–734.
46. Pham, C. L. L.; Kwan, A. H.; Sunde, M. Functional Amyloid: Widespread in Nature, Diverse in Purpose. *Essays Biochem.* **2014**, *56*, 207–219.
47. Baldwin, A. J.; Bader, R.; Christodoulou, J.; MacPhee, C. E.; Dobson, C. M.; Barker, P. D. Cytochrome Display on Amyloid Fibrils. *J. Am. Chem. Soc.* **2006**, *128*, 2162–2163.
48. Pilkington, S. M.; Roberts, S. J.; Meade, S. J.; Gerrard, J. A. Amyloid Fibrils as a Nanoscaffold for Enzyme Immobilization. *Biotechnol. Prog.* **2010**, *26*, 93–100.
49. Li, C.; Adamcik, J.; Mezzenga, R. Biodegradable Nanocomposites of Amyloid Fibrils and Graphene with Shape-Memory and Enzyme-Sensing Properties. *Nat. Nanotechnol.* **2012**, *7*, 421–427.
50. Li, C. X.; Born, A. K.; Schweizer, T.; Zenobi-Wong, M.; Cerruti, M.; Mezzenga, R. Amyloid-Hydroxyapatite Bone Biomimetic Composites. *Adv. Mater.* **2014**, *26*, 3207–3212.
51. Reynolds, N. P.; Charnley, M.; Mezzenga, R.; Hartley, P. G. Engineered Lysozyme Amyloid Fibril Networks Support Cellular Growth and Spreading. *Biomacromolecules* **2014**, *15*, 599–608.
52. Udomprasert, A.; Bongiovanni, M. N.; Sha, R. J.; Sherman, W. B.; Wang, T.; Arora, P. S.; Canary, J. W.; Gras, S. L.; Seeman, N. C. Amyloid Fibrils Nucleated and Organized by DNA Origami Constructions. *Nat. Nanotechnol.* **2014**, *9*, 537–541.
53. Shimanovich, U.; Efimov, I.; Mason, T. O.; Flagmeier, P.; Buell, A. K.; Gedanken, A.; Linse, S.; Akerfeldt, K. S.; Dobson, C. M.; Weitz, D. A.; et al. Protein Microgels from Amyloid Fibril Networks. *ACS Nano* **2015**, *9*, 43–51.
54. Seiffert, S. Small but Smart: Sensitive Microgel Capsules. *Angew. Chem., Int. Ed.* **2013**, *52*, 11462–11468.
55. Nisisako, T.; Torii, T. Microfluidic Large-Scale Integration on a Chip for Mass Production of Monodisperse Droplets and Particles. *Lab Chip* **2008**, *8*, 287–293.
56. Mazutis, L.; Gilbert, J.; Ung, W. L.; Weitz, D. A.; Griffiths, A. D.; Heyman, J. A. Single-Cell Analysis and Sorting Using Droplet-Based Microfluidics. *Nat. Protoc.* **2013**, *8*, 870–891.
57. Fischlechner, M.; Schaerli, Y.; Mohamed, M. F.; Patil, S.; Abell, C.; Hollfelder, F. Evolution of Enzyme Catalysts Caged in Biomimetic Gel-Shell Beads. *Nat. Chem.* **2014**, *6*, 791–796.
58. Wang, Y. Q.; Buell, A. K.; Wang, X. Y.; Welland, M. E.; Dobson, C. M.; Knowles, T. P.; Perrett, S. Relationship between Prion Propensity and the Rates of Individual Molecular Steps of Fibril Assembly. *J. Biol. Chem.* **2011**, *286*, 12101–12107.
59. Knowles, T. P. J.; Waudby, C. A.; Devlin, G. L.; Cohen, S. I. A.; Aguzzi, A.; Vendruscolo, M.; Terentjev, E. M.; Welland, M. E.; Dobson, C. M. An Analytical Solution to the Kinetics of Breakable Filament Assembly. *Science* **2009**, *326*, 1533–1537.
60. Chen, L.; Chen, L. J.; Wang, H. Y.; Wang, Y. Q.; Perrett, S. Deletion of a Ure2 C-Terminal Prion-Inhibiting Region Promotes the Rate of Fibril Seed Formation and Alters Interaction with Hsp40. *Protein. Eng. Des. Sel.* **2011**, *24*, 69–78.
61. Xu, L. Q.; Wu, S.; Buell, A. K.; Cohen, S. I. A.; Chen, L. J.; Hu, W. H.; Cusack, S. A.; Itzhaki, L. S.; Zhang, H.; Knowles, T. P. J., et al. Influence of Specific Hsp70 Domains on Fibril Formation of the Yeast Prion Protein Ure2. *Philos. T. R. Soc. B* **2013**, *368*.
62. Bai, M.; Zhou, J. M.; Perrett, S. The Yeast Prion Protein Ure2 Shows Glutathione Peroxidase Activity in Both Native and Fibrillar Forms. *J. Biol. Chem.* **2004**, *279*, 50025–50030.

63. Varde, N. K.; Pack, D. W. Microspheres for Controlled Release Drug Delivery. *Expert. Opin. Biol. Th.* **2004**, *4*, 35–51.
64. Barabino, R. C.; Gray, D. N.; Keyes, M. H. Coupled Reactions of Immobilized Enzymes and Immobilized Substrates - Clinical Application as Exemplified by Amylase Assay. *Clin. Chem.* **1978**, *24*, 1393–1398.
65. Tischer, W.; Wedekind, F. Immobilized Enzymes: Methods and Applications. *Top. Curr. Chem.* **1999**, *200*, 95–126.
66. Tumarkin, E.; Tzadu, L.; Csaszar, E.; Seo, M.; Zhang, H.; Lee, A.; Peerani, R.; Purpura, K.; Zandstra, P. W.; Kumacheva, E. High-Throughput Combinatorial Cell Co-Culture Using Microfluidics. *Integr. Biol.* **2011**, *3*, 653–662.
67. Guo, M. T.; Rotem, A.; Heyman, J. A.; Weitz, D. A. Droplet Microfluidics for High-Throughput Biological Assays. *Lab Chip* **2012**, *12*, 2146–2155.
68. Dolatshahi-Pirouz, A.; Nikkhah, M.; Gaharwar, A. K.; Hashmi, B.; Guermani, E.; Aliabadi, H.; Camci-Unal, G.; Ferrante, T.; Foss, M.; Ingber, D. E.; et al. A Combinatorial Cell-Laden Gel Microarray for Inducing Osteogenic Differentiation of Human Mesenchymal Stem Cells. *Sci. Rep.* **2014**, *4*, 3896.
69. McDonald, J. C.; Whitesides, G. M. Poly(dimethylsiloxane) as a Material for Fabricating Microfluidic Devices. *Acc. Chem. Res.* **2002**, *35*, 491–499.
70. Qin, D.; Xia, Y. N.; Whitesides, G. M. Soft Lithography for Micro- and Nanoscale Patterning. *Nat. Protoc.* **2010**, *5*, 491–502.